Research Article Vol. 17, No. 4 / 1 Apr 2026 / Biomedical Optics Express 1673
Biomedical Optics EXPRESS

Quantitative rFRC-based evaluation of computational resolution enhancement in in vivo two-photon subcellular imaging

SAEED BOHLOOLI DARIAN,[1] JEONGMIN OH,[2] AND JUN KI KIM[2,*]

[1]Department of Convergence Medicine, Brain Korea 21 Project, University of Ulsan, College of Medicine, Seoul, 05505, Republic of Korea
[2]Biomedical Engineering Research Center, Asan Medical Center, Seoul 05505, Republic of Korea
*kim@amc.seoul.kr

Abstract: Intravital imaging with conventional microscopy faces major technical barriers, including limited spatial resolution, high background noise, and motion artifacts caused by physiological activity such as respiration and heartbeat. To visualize subcellular structures such as mitochondria and dynamic processes like autophagy in vivo, we developed an integrated imaging framework that combines two-photon microscopy with tissue stabilization, denoising, and a computational resolution enhancement algorithm. This approach enables high-fidelity visualization of fine intracellular features in living tissues, revealing structural details that typically remain obscured in standard intravital imaging. By improving both signal quality and spatial precision, the platform expands the capacity of in vivo microscopy to investigate rapid organelle dynamics and stress-induced cellular responses.

1. Introduction

Understanding molecular and cellular processes within the intact physiological environment of living organisms remains a central goal in modern biological research [1,2]. Intravital microscopy [3–5] has become an indispensable tool toward this objective, providing the means to visualize tissues in situ and monitor dynamic interactions at subcellular to tissue scales [6]. Despite its powerful capabilities, the performance of intravital imaging is often compromised by intrinsic optical and mechanical limitations [7,8]. Light scattering in heterogeneous tissues degrades spatial resolution [9] and background autofluorescence reduces image contrast. In addition, persistent physiological motion, driven by respiration, cardiac activity, and vascular pulsation introduces distortions that obscure fine structural features [10]. These limitations significantly hinder studies that require nanoscale resolution, especially those aimed at capturing rapid and transient biological events in vivo. Effective strategies to overcome these technical barriers must integrate improvements in mechanical stabilization with advanced computational approaches capable of extracting reliable structural information from noisy and motion-affected datasets [11].

Mitochondria [12–14] represent a biologically and clinically critical target for such enhanced imaging strategies. As central regulators of oxidative metabolism, redox homeostasis, and stress adaptation, their morphology and spatial organization reflect the functional state of the cell [15,16]. Mitochondrial networks undergo rapid remodeling in response to pathological stimuli, including toxic injury, nutrient imbalance, and metabolic stress [17]. However, resolving these morphological transitions in vivo has remained technically challenging due to the resolution limits of conventional intravital microscopy and the deleterious effects of motion artifacts during prolonged imaging.

Autophagy [18–21] constitutes another essential cellular process that is particularly demanding to visualize in living tissue. Through the sequential formation, expansion, and trafficking of autophagosomes [22], the autophagic pathway mediates the selective degradation of cytoplasmic

#589972 https://doi.org/10.1364/BOE.589972
Journal © 2026 Received 9 Jan 2026; revised 3 Mar 2026; accepted 3 Mar 2026; published 5 Mar 2026

Biomedical Optics EXPRESS

components and damaged organelles. Autophagosomes are small, short-lived structures that require high spatial and temporal resolution for accurate detection, and intravital methods have historically lacked the ability to capture their nanoscale dynamics under physiological or pathological conditions [23].

In this work, we present an integrated imaging framework that combines two-photon microscopy [24–26] with computational enhancement to address these long-standing limitations. Our approach incorporates mechanical stabilization of the imaging tissue, trained denoising model to suppress background noise, and enhanced Super-Resolution Radial Fluctuations (eSRRF) [27] to surpass diffraction-limited resolution by leveraging temporal fluorescence fluctuations. In live mouse models, this framework enables the visualization of mitochondrial remodeling in ethanol-induced liver injury [28,29] of Dendra2 mice and the characterization of autophagosome formation in starved GFP-LC3 reporter mice [30,31].

Overall, our findings demonstrate that the integration of stabilization techniques with computational enhancement can substantially improve the quality and interpretability of intravital images. The resulting framework enables reliable visualization of subcellular structures within living tissue and provides a practical means for extracting nanoscale information from physiologically active environments. It further offers a powerful tool for dissecting cellular adaptation in vivo. The methodology presented here is broadly compatible with standard imaging systems and can be readily adapted to other organs, experimental models, and biological questions, contributing to the continued expansion of high-resolution intravital microscopy.

2. Materials and methods

2.1. Animal experiments

all experiments were conducted in adherence to NIH Guidelines and received approval from the Institutional Animal Care and Use Committee at Asan Medical Center. Transgenic Dendra2 and GFP-LC3 mice were employed as in vivo models for high-resolution imaging of mitochondrial dynamics and autophagic activity, respectively. To preserve tissue architecture and physiological function during imaging, a custom 3D-printed portable imaging window was affixed to the objective lens, applying gentle negative pressure to immobilize the tissue and minimize motion artifacts.

Following anesthesia, for liver imaging, a small abdominal incision allowed direct exposure of hepatocytes, taking care to avoid disruption of surrounding structures. For skeletal muscle imaging, the skin overlying the thigh was carefully reflected to expose the quadriceps muscle. Post-imaging, all incisions were precisely sutured and sterilized, and animals were maintained on a heated recovery pad to preserve normothermia and support rapid recovery. Mice were continuously monitored until fully stabilized before being returned to their cages.

After acquisition of baseline control data, to investigate autophagic responses under metabolic stress, GFP-LC3 mice were subjected to a 48-hour starvation protocol with ad libitum access to water. Following this period, liver and muscle tissues were re-exposed and imaged under identical conditions to directly assess starvation-induced autophagosome formation. In a separate cohort, Dendra2 mice received a single oral gavage of ethanol (70%, 4 g/kg) to induce acute liver injury. Liver imaging was performed immediately to obtain the control data and again 3 hours post-administration to capture ethanol-induced mitochondrial morphological changes in vivo.

2.2. Imaging

Intravital imaging was performed using a conventional two-photon microscope (IVM-MS, IVIM Technology, Korea) equipped with a Ti:Sapphire laser tuned to 920 nm (Coherent Inc., Santa Clara, USA). Fluorescence signals were simultaneously detected using high-sensitivity, broadband emission detectors (185–760 nm) to enable precise visualization of subcellular structures.

Biomedical Optics EXPRESS

Imaging was conducted with a high-magnification objective lens (100×, 1.45 NA, Olympus, Japan), providing the spatial resolution required to resolve fine intracellular features in vivo.

2.3. Image analysis

Image processing and analysis were performed using Fiji [32]. Raw image stacks were first subjected to background noise suppression using a self-supervised denoising approach implemented via the Noise2Void (N2 V) plugin [33], effectively enhancing signal fidelity without introducing artificial structures. To correct for residual motion and physiological artifacts, image stacks underwent frame-to-frame registration, ensuring stable and consistent datasets for downstream analyses.

Following preprocessing, eSRRF analysis was applied to achieve computational resolution improvement. Optimal eSRRF reconstruction values were obtained through a systematic parameter sweep, fine-tuning sensitivity, and ring radius settings to maximize structural detail while minimizing reconstruction artifacts. The performance of this processing pipeline was quantitatively evaluated by comparing conventional two-photon images with eSRRF-enhanced datasets using rolling Fourier ring correlation (rFRC) analysis with 1/7 threshold and the default block size of 64 pixels, via the PANELJ plugin [34]. This analysis showed substantial improvement in effective spatial resolution and organelle visualization, representing computational estimates of structural resolvability rather than direct optical resolution measurements. Importantly, the resolution values reported here represent effective, computationally estimated resolution and reflect enhanced image separability and structural discrimination rather than direct measurements of the optical diffraction limit.

Autophagosome identification was performed using a standardized workflow applied to all datasets. After motion correction and denoising, images were analyzed using fixed normalization and thresholding parameters. LC3-positive autophagosomes were defined as discrete puncta within a specified size and circularity range, and were required to persist across consecutive frames to reduce noise-related false positives. All detection settings were kept constant across groups to avoid analysis bias.

3. Results

3.1. Visualization enhancement

A protocol was established for intravital imaging that combines effective tissue stabilization with two-photon microscopy to support long-term, high-resolution visualization of subcellular architecture in living animals. This integrated approach minimizes motion-induced distortions and maintains stable imaging conditions over extended sessions, enabling reliable nanoscale assessment of dynamic structures. Using this platform, mitochondria were imaged in a model of alcohol-induced liver injury, and autophagosomes were visualized in a starvation-triggered autophagy model, confirming its applicability across distinct biological contexts and fluorescent labeling strategies. Figure 1 illustrates the overall imaging and processing workflow, showing how raw, noise-affected intravital images of subcellular structures are progressively refined through computational processing to yield markedly clearer, high-resolution representations suitable for quantitative analysis.

Figure 2 presents a comparison of control liver images from GFP-LC3 and Dendra2 mice before and after processing, demonstrating a clear enhancement in structural definition. The processing pipeline yields sharper nuclear boundaries and markedly improved visualization of subcellular features. Before applying eSRRF-based image enhancement, key algorithm parameters were systematically optimized. A comprehensive parameter sweep was performed to evaluate their impact on image quality. As shown in Fig. 2(a), Analysis of the resolution sweep and QnR maps was performed across parameter combinations. The resolution sweep

Biomedical Optics EXPRESS

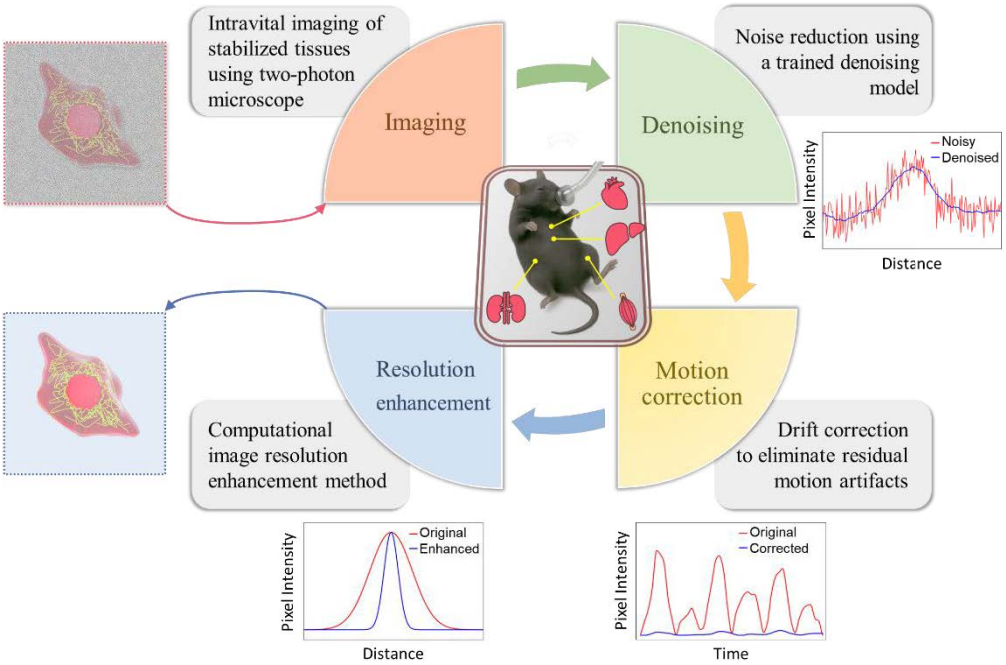

Fig. 1. Schematic overview of the image processing pipeline. Initial raw intravital images, affected by motion and background noise, are sequentially corrected through drift correction and a self-supervised denoising model before undergoing computational resolution enhancement with the eSRRF algorithm. The integrated workflow produces high-fidelity, high-resolution reconstructions that reveal subcellular structures with substantially improved clarity.

map illustrates how estimated resolution varies with radius and sensitivity, but was used only as a complementary reference because higher nominal resolution did not always correspond to stable, artifact-free reconstructions. Parameter selection was therefore based primarily on the QnR metric, with the highest QnR value observed at a radius of 2 and a sensitivity of 0.5; these settings were used for subsequent eSRRF processing. Improving image quality is particularly critical in GFP-LC3 mice (Fig. 2(b)), where the weak GFP signal from autophagosomes, together with low tissue autofluorescence and high background noise, results in poor contrast and obscures fine structural details in raw intravital images. In Dendra2 mice (Fig. 2(c)), the enhanced images reveal individual mitochondria with markedly improved clarity and separation. Pixel intensity extracted from depicted profile lines and SNR measurements provide further quantitative support for these improvements, demonstrating clearer peak separation and increased signal-to-noise ratio after processing, consistent with enhanced structural separability.

To further demonstrate the effect of the proposed resolution enhancement strategy, spatial resolution was quantitatively evaluated before and after image processing. Figure 3(a) shows an enhanced hepatocyte image from the Dendra2 mouse together with the corresponding rFRC map and a merged visualization highlighting regions of varying image quality. Local resolution was assessed using rFRC maps, which report locally estimated effective resolution rather than a direct fidelity metric. Lower values correspond to improved resolvability and were interpreted based on spatial consistency rather than a fixed threshold. Figure 3(b) presents a direct comparison of the original and processed liver cell images within a single composite view, and Fig. 3(c) summarizes the corresponding rFRC measurements. The analysis demonstrates improved structural separability after processing, supported by clearer peak distinction in line profiles and

Biomedical Optics EXPRESS

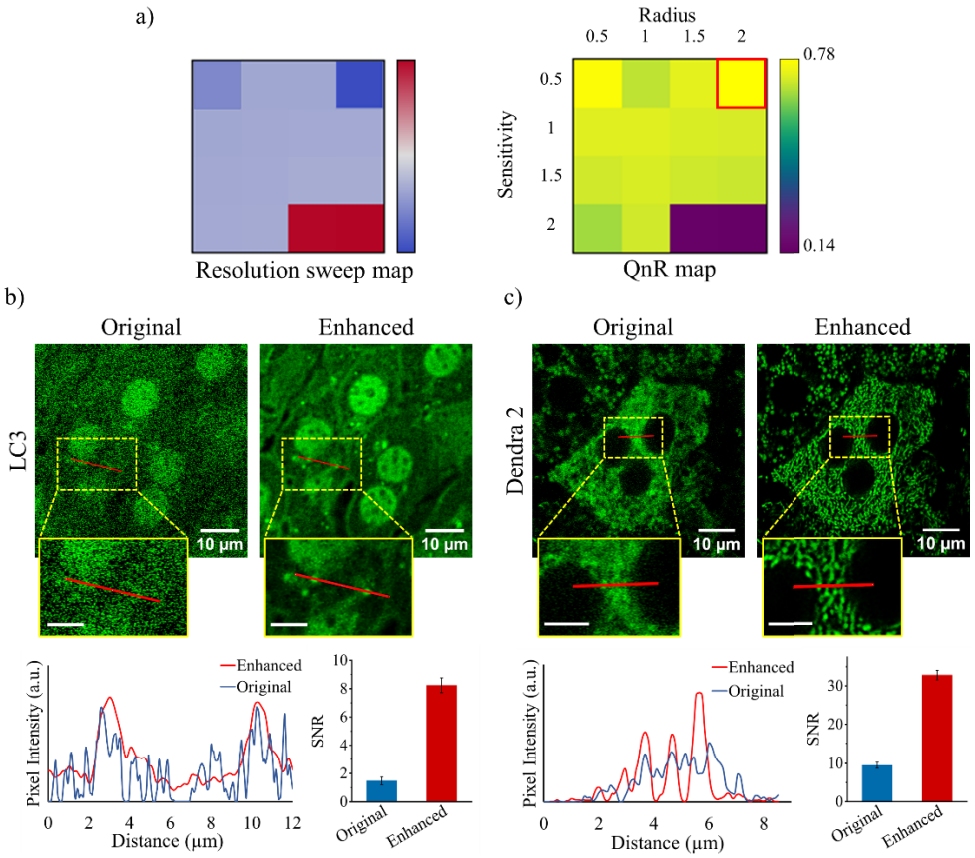

Fig. 2. Original and enhanced liver images from LC3 and Dendra2 mice. (a) Resolution sweep and QnR maps obtained during eSRRF parameter optimization. The resolution sweep shows estimated resolution trends, while QnR reflects reconstruction quality. Parameters were selected based on the QnR maximum. (b) and (c) The original images and their processed counterparts which illustrate substantial gains in contrast, sharper delineation of structural boundaries, and improved visibility of fine subcellular details. SNR plots further demonstrate reduced background noise and improved structural separability following computational processing in LC3 and Dendra2 mice. (Scale bar insets, 5 μm)

increased local SNR. On average, the effective resolution estimate improved from approximately 587.6 nm in the original images to 108.4 nm following enhancement. These values reflect computationally derived effective resolution and not the optical diffraction limit.

3.2. Autophagy and mitochondria under metabolic stress

To evaluate the applicability of the workflow in biologically relevant contexts, we applied it to experimentally induced models of metabolic stress. In GFP-LC3 mice, baseline images were first acquired under normal physiological conditions. The mice then underwent a 48-hour fasting regimen to induce nutrient-deprivation–driven autophagic responses. After the fasting period, the liver and thigh muscle were re-exposed and imaged under the same intravital conditions, allowing direct comparison of starvation-induced cellular changes with their corresponding baseline states. High-resolution reconstructions of muscle fibers and hepatocytes (Fig. 4(a)) revealed a pronounced increase in both the number and size of LC3-positive autophagosomes in the starved group (Fig. 4(b)), consistent with robust autophagy activation during nutrient

Biomedical Optics EXPRESS

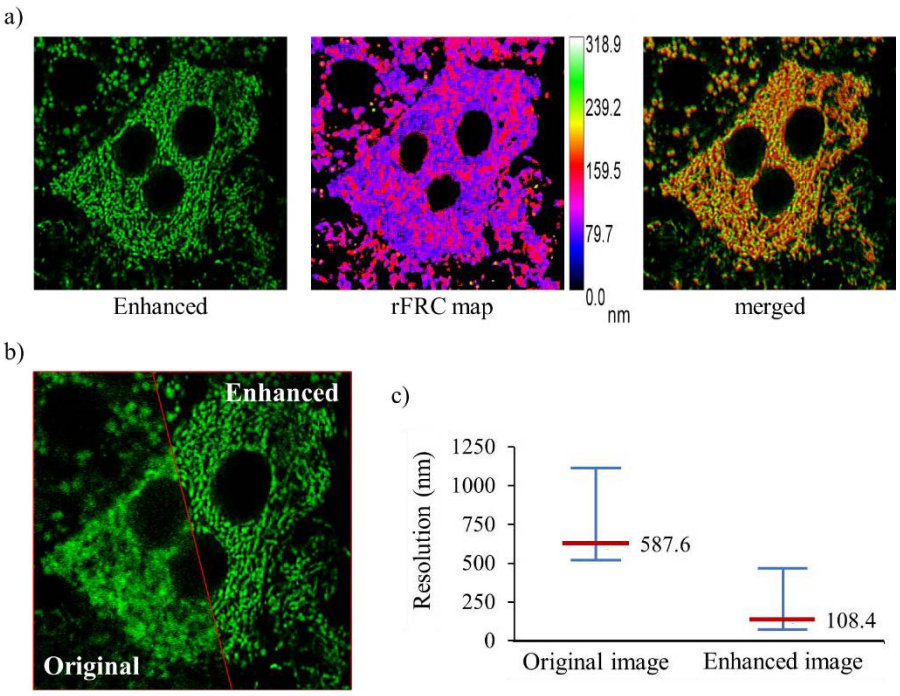

Fig. 3. Resolution improvement in intravital liver imaging. (a) A representative single-hepatocyte image showing the enhanced result, the corresponding rFRC map derived from spatial resolution investigation, and a merged visualization highlighting regions with differing resolution and image quality. (b) Direct side-by-side composite of the original and enhanced images, illustrating the visual impact of the computational enhancement pipeline. (c) Quantitative comparison of spatial resolution before and after processing based on rFRC analysis, demonstrating the improvement in effective spatial resolution. Minimum, maximum, and mean rFRC-derived values are shown to quantify the extent of resolution enhancement across the dataset.

deprivation. All datasets were processed using the same computational parameters, ensuring that observed differences reflect starvation-induced biological changes rather than variations introduced by image enhancement.

In parallel, mitochondrial morphology was assessed in Dendra2 mice following acute ethanol exposure. As shown in Fig. 4(c), ethanol treatment produced clear alterations in mitochondrial architecture, and quantitative analysis (Fig. 4(d)) demonstrated significant shifts in mitochondrial length and circularity, indicative of enhanced fission and structural fragmentation.

Together, these findings show that metabolic stress, whether triggered by nutrient deprivation or ethanol challenge, disrupts cellular homeostasis by increasing autophagic activity and promoting the fragmentation of vulnerable mitochondria in vivo. These observations reflect coordinated stress-response pathways that reshape subcellular architecture under physiological pressure.

4. Discussion

The present study introduces a computational strategy for improving intravital optical imaging quality without requiring hardware modifications or specialized microscopy components. The workflow integrates mechanical tissue stabilization, self-supervised denoising, motion correction, and eSRRF-based resolution enhancement to extract high-fidelity structural information from image sequences that are inherently affected by physiological motion and low signal levels.

Biomedical Optics EXPRESS

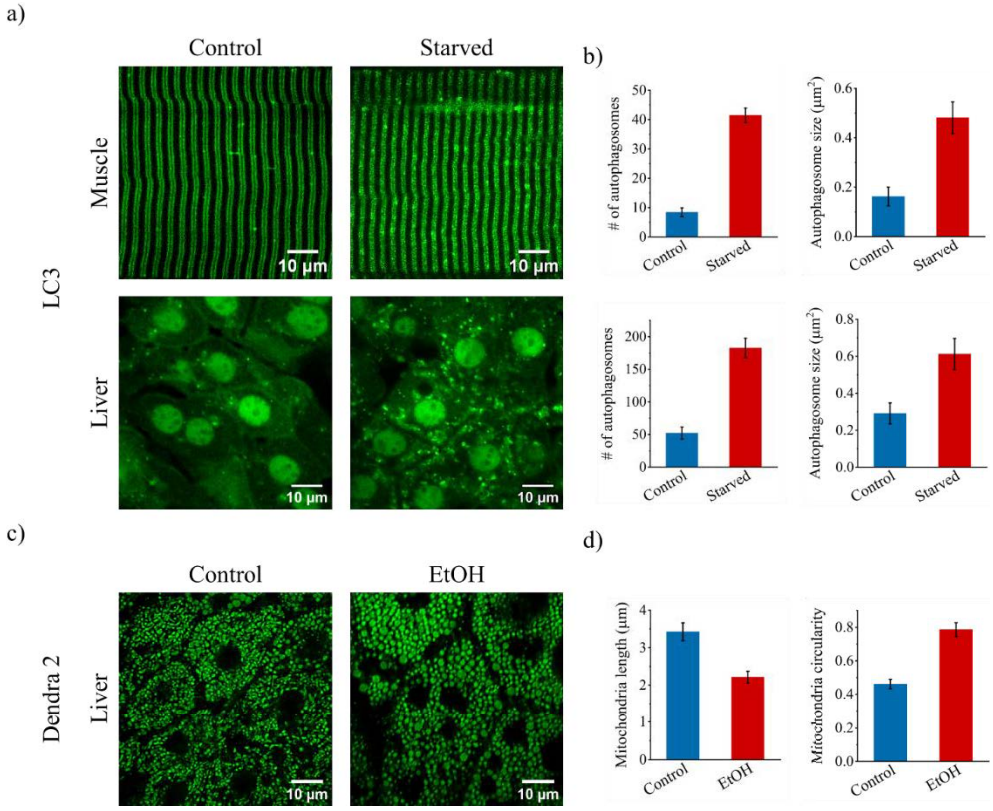

Fig. 4. Intravital visualization of starvation- and ethanol-induced subcellular responses in vivo. (a) High-resolution images of hepatocytes and muscle fibers from control and 48-hour starved GFP-LC3 mice. (b) Quantitative comparison of starvation effects on autophagosome number and size. (c) Mitochondrial morphology in the livers of Dendra2 mice before and after ethanol treatment. (d) Quantitative analysis of ethanol-induced changes in mitochondrial length and circularity in hepatocytes.

Together, these steps address two persistent challenges in intravital microscopy: tissue instability and limited signal-to-noise ratios that obscure fine subcellular features.

Within this pipeline, each component serves a distinct role. Mechanical stabilization primarily reduces large-scale tissue displacement, which is a major source of defocus and misalignment during in vivo imaging. Following stabilization, the self-supervised denoising model improves image clarity by learning noise statistics directly from the acquired data, without requiring ground-truth references, resulting in an approximately three- to four-fold increase in signal-to-noise ratio as confirmed by quantitative analysis. Residual frame-to-frame motion is subsequently corrected through computational registration to generate temporally consistent datasets. Finally, eSRRF reconstruction is applied to enhance effective spatial resolution, with parameters conservatively selected based on QnR optimization to minimize reconstruction artifacts. Enhanced features were verified to correspond to structures present in the original data, supporting the reliability of the reconstructed images. rFRC analysis supported this improvement, indicating that the estimated effective resolution improved from approximately 587 nm in the raw images to nearly 108 nm in the enhanced versions; these values reflect computationally derived structural resolvability rather than direct optical resolution. To prevent from algorithmic consistency, we interpret

Biomedical Optics EXPRESS

these estimates alongside visual and profile-based separability analyses rather than as standalone measures.

The workflow demonstrated strong performance across two distinct biological models. In ethanol-treated Dendra2 mice, acute alcohol exposure is known to disrupt hepatocyte homeostasis and perturb mitochondrial function. In response to this form of metabolic stress, mitochondria undergo dynamic remodeling, and the transition from elongated to more circular structures observed in our analysis is consistent with increased fission activity, a characteristic cellular response to damage. In the starvation model, GFP-LC3 mice exhibited a substantial increase in autophagosome formation, reflecting activation of autophagy as a compensatory mechanism for maintaining cellular energy balance. Together, these findings demonstrate that the computational pipeline enables visualization of biologically meaningful changes in subcellular organization that are often masked in conventional intravital datasets.

Although the two models differ in tissue type, fluorescent labeling strategy, and biological response, the processing pipeline consistently improved structural clarity. This consistency supports its extension to the study of dynamic subcellular processes, including mitochondrial remodeling, autophagosome formation, vesicle trafficking, and cytoskeletal organization. The present implementation is optimized for enhancing spatial resolution and structural delineation; while temporal relationships are preserved at the scale of the acquired image sequences. The improved signal stability and effective resolution enable more confident morphological analysis and may reduce reliance on invasive validation techniques such as fixation or immunostaining, which can distort native cellular structures.

A major strength of this approach lies in its flexibility. Because all enhancements are implemented through software, the method can be readily applied across a wide range of intravital imaging systems without additional cost, custom optics, or acquisition modifications. This accessibility positions the framework as a practical option for laboratories seeking to extend the analytical power of existing instruments while avoiding substantial technical or financial barriers.

Future work will extend this strategy to organs with challenging imaging environments, including the lung, kidney, and beating heart, to evaluate performance under more complex motion conditions. Additional development may also incorporate adaptive or automated parameter selection tailored to tissue type, imaging depth, or fluorophore characteristics, which would enhance reproducibility and reduce user variability. As computational imaging continues to advance, software-based enhancement approaches such as the one presented here are expected to play an increasingly important role in producing richer and more informative intravital measurements of biological processes in living systems.

5. Conclusion

We established an adjustable intravital imaging platform that integrates two-photon microscopy with computational resolution enhancement to address longstanding limitations in live-animal imaging. Through the combination of a gentle tissue-stabilization strategy, a self-supervised denoising model, and an eSRRF-based super-resolution algorithm, the system effectively reduces motion artifacts and improves signal quality while avoiding the need for specialized optical hardware. This framework enabled high-resolution visualization and quantitative assessment of mitochondrial remodeling and autophagic activity in living animals exposed to physiological and pathological challenges, including ethanol treatment and prolonged starvation. The overall approach offers a practical and reproducible route for probing dynamic subcellular processes in vivo and holds significant potential for advancing studies of disease mechanisms, metabolic regulation, and therapeutic responses.

Funding. National Research Foundation of Korea (RS-2024-00450201, RS-2025-25407039).

Disclosures. The authors declare no conflicts of interest.

Biomedical Optics EXPRESS

Data availability. The datasets used and/or analyzed during the current study are available from the corresponding author on a request.

References

1. T. F. Massoud and S. S. Gambhir, "Molecular imaging in living subjects: seeing fundamental biological processes in a new light," Genes Dev. **17**(5), 545–580 (2003).
2. M. Shvedunova and A. Akhtar, "Modulation of cellular processes by histone and non-histone protein acetylation," Nat. Rev. Mol. Cell Biol. **23**(5), 329–349 (2022).
3. A. Masedunskas, O. Milberg, N. Porat-Shliom, *et al.*, "Intravital microscopy: a practical guide on imaging intracellular structures in live animals," Bioarchitecture **2**(5), 143–157 (2012).
4. C. A. Dawson, S. N. Mueller, G. J. Lindeman, *et al.*, "Intravital microscopy of dynamic single-cell behavior in mouse mammary tissue," Nat. Protoc. **16**(4), 1907–1935 (2021).
5. E. Dondossola and P. Friedl, "Host responses to implants revealed by intravital microscopy," Nat. Rev. Mater. **7**(1), 6–22 (2021).
6. T. J. Bechtel, T. Reyes-Robles, O. O. Fadeyi, *et al.*, "Strategies for monitoring cell–cell interactions," Nat. Chem. Biol. **17**(6), 641–652 (2021).
7. C. L. Scheele, D. Herrmann, E. Yamashita, *et al.*, "Multiphoton intravital microscopy of rodents," Nat. Rev. Methods Primers **2**(1), 89 (2022).
8. Y. Wang, F. Heymann, M. Peiseler, *et al.*, "Intravital imaging: dynamic insights into liver immunity in health and disease," Gut **73**(8), 1364–1375 (2024).
9. R. Chen, S. Peng, Q. Xia, *et al.*, "Intravital observation of high-scattering and dense-labeling hepatic tissues using multi-photon fluorescence microscopy," J. Biophotonics **17**(6), e202300477 (2024).
10. M. J. Pittet and R. Weissleder, "Intravital imaging," Cell **147**(5), 983–991 (2011).
11. S. B. Darian, J. Oh, B. Paulson, *et al.*, "Multiphoton intravital microscopy in small animals of long-term mitochondrial dynamics based on super-resolution radial fluctuations," Opto-Electron. Adv. **8**, 240311 (2025).
12. E. L. Mills, B. Kelly, L. A J O'Neill, *et al.*, "Mitochondria are the powerhouses of immunity," Nat. Immunology **18**(5), 488–498 (2017).
13. S. J. Annesley and P. R. Fisher, "Mitochondria in health and disease," (MDPI, 2019), p. 680.
14. H. M. McBride, M. Neuspiel, S. Wasiak, *et al.*, "Mitochondria: more than just a powerhouse," Curr. Biol. **16**(14), R551–R560 (2006).
15. L. D. Zorova, V. A. Popkov, E. Y. Plotnikov, *et al.*, "Mitochondrial membrane potential," Anal. Biochem. **552**, 50–59 (2018).
16. A. J. Duraisamy, G. Mohammad, R. A. Kowluru, *et al.*, "Mitochondrial fusion and maintenance of mitochondrial homeostasis in diabetic retinopathy," Biochimica et Biophysica Acta (BBA)-Molecular Basis of Dis. **1865**(6), 1617–1626 (2019).
17. P. Prasun, I. Ginevic, K. Oishi, *et al.*, "Mitochondrial dysfunction in nonalcoholic fatty liver disease and alcohol related liver disease," Transl. Gastroenterol. Hepatol. **6**, 4 (2021).
18. Y. Aman, T. Schmauck-Medina, M. Hansen, *et al.*, "Autophagy in healthy aging and disease," Nat. Aging **1**(8), 634–650 (2021).
19. T. Ichimiya, T. Yamakawa, T. Hirano, *et al.*, "Autophagy and Autophagy-Related Diseases: A Review," Int. J. Mol. Sci. **21**(23), 8974 (2020).
20. R. Cursio, P. Colosetti, J. Gugenheim, *et al.*, "Autophagy and Liver Ischemia-Reperfusion Injury," BioMed Res. Int. **2015**, 1–16 (2015).
21. S. Saha, D. P. Panigrahi, S. Patil, *et al.*, "Autophagy in health and disease: A comprehensive review," Biomed. Pharmacother. **104**, 485–495 (2018).
22. H. Nakatogawa, "Mechanisms governing autophagosome biogenesis," Nat. Rev. Mol. Cell Biol. **21**(8), 439–458 (2020).
23. S. W. Ryter, S. M. Cloonan, A. M. K. Choi, *et al.*, "Autophagy: A Critical Regulator of Cellular Metabolism and Homeostasis," Molecules and Cells **36**(1), 7–16 (2013).
24. F. Helmchen and W. Denk, "Deep tissue two-photon microscopy," Nat. Methods **2**(12), 932–940 (2005).
25. M. Rubart, "Two-Photon Microscopy of Cells and Tissue," Circ. Res. **95**(12), 1154–1166 (2004).
26. H. J. Edenberg and J. N. McClintick, "Alcohol dehydrogenases, aldehyde dehydrogenases, and alcohol use disorders: a critical review," Alcoholism: Clin. Experiment. Res. **42**(12), 2281–2297 (2018).
27. R. F. Laine, H. S. Heil, S. Coelho, *et al.*, "High-fidelity 3D live-cell nanoscopy through data-driven enhanced super-resolution radial fluctuation," Nat. Methods **20**(12), 1949–1956 (2023).
28. S. Jeon and R. Carr, "Alcohol effects on hepatic lipid metabolism," J. Lipid Res. **61**(4), 470–479 (2020).
29. R. S. O'shea, S. Dasarathy, A. J. McCullough, *et al.*, "Alcoholic liver disease," Hepatology **51**(1), 307–328 (2010).
30. J. A. Oliva Trejo, I. Tanida, C. Suzuki, *et al.*, "Characterization of starvation-induced autophagy in cerebellar Purkinje cells of pHluorin-mKate2-human LC3B transgenic mice," Sci. Rep. **10**(1), 9643 (2020).
31. Y. Feng, Y. Chen, X. Wu, *et al.*, "Interplay of energy metabolism and autophagy," Autophagy **20**(1), 4–14 (2024).
32. J. Schindelin, A.-C. Ignacio, F. Erwin, *et al.*, "Fiji: an open-source platform for biological-image analysis," Nat. Methods **9**(7), 676–682 (2012).

Biomedical Optics EXPRESS

33. S. M. H. Varun, Y. Zhang, and Y. Zhu, "Fluorescence Microscopy Denoising (FMD) dataset," University of Notre Dame (2020).
34. W. Zhao, X. Huang, J. Yang, *et al.*, "Quantitatively mapping local quality of super-resolution microscopy by rolling Fourier ring correlation," Light: Sci. Appl. **12**(1), 298 (2023).